JTTEE5 10:359-366

Investigation of Particle In-flight Characteristics during Atmospheric Plasma Spraying of Yttria Stabilized ZrO_2: Part 2. Modeling

Per Nylén, Martin Friis, Anita Hansbo, and Lars Pejryd

(Submitted 25 October 1999)

Yttria stabilized ZrO_2 particle in-flight characteristics in an Ar-H_2 atmospheric plasma jet have been studied using analytical and experimental techniques. In the previous article,[1] the primary gas flow, plasma composition, current, and powder feed rate were systematically varied and particle surface temperatures, velocities, and size distributions measured and statistically analyzed. In this paper, a mathematical model for the plasma flow and particle characteristics is presented. Model predictions are compared with the experimental results in Ref 1 and a reasonable correlation is found. A statistical investigation (composite cubic face (CCF)) is performed on the particle predictions, giving fast and simple relationships between gun parameters and particle in-flight properties. The statistical and theoretical models that are presented here combine to form a powerful and cost-effective tool, which can be used in the evaluation and optimization of spray parameters off-line.

Keywords particle temperature, particle velocity, plasma modeling, plasma spraying, yttria stabilized ZrO_2

1. Introduction

The plasma spray process is composed of three separate processes: the plasma generation, the plasma/particle interaction, and the formation of the coating. The characteristics of the particles prior to impact, such as velocity and particle state (*i.e.*, partly or fully molten), are probably the most important factors influencing the microstructure and properties of the coating.

Our purpose is to investigate possible relations between process parameters, such as gas flow and energy input, on the one hand, and particle properties, on the other. The experimental study and statistical evaluation of the particle behavior is the subject of a companion article (Part I, *cf.* Ref 1). In the present work, the temperature, state, and velocity of yttria stabilized ZrO_2 particles are predicted by means of numerical modeling. Of particular interest is whether the model presented is capable of predicting correct trends when operation conditions are varied within a limited range.

Modern on-line measurement systems[2] have the potential to become efficient diagnostic tools for controlling the plasma spray process. To develop a control strategy, a simple and computationally fast model linking a few spray gun parameters with particle in-flight characteristics is needed. We expect any simple model to be dependent on the particular spray situation and to be valid only in a small window in the parameter space. To reduce the need for expensive experiments, it is important to evaluate the possibility to use computer simulations to obtain simple parameter relationships. Such an investigation is therefore performed using a composite cubic face (CCF) experimental design.[3]

A commercial code is used for the numerical solution of the incompressible Navier-Stokes equations to simulate the plasma flow. In these calculations, a mass fraction conservation equation takes interdiffusion effects between plasma and surrounding air into account. An in-house code is used for the particle property calculations. Allowance has been made for noncontinuum effects, internal heat conduction, phase changes, reduced heat transfer due to particle vaporization, and the effects of variable plasma properties in the plasma boundary layer.

The discrepancy between predictions and measurements is about 5 to 10%, but we still conclude that the model is able to predict trends fairly accurately and that the method described might be a cost-effective tool to increase the reproducibility of the plasma spray process.

2. Calculations of Plasma Jet Characteristics

The numerical simulations are made using the Fluent commercial CFD code (Fluent Incorporated, Centerra Resource Park, Lebanon, USA). It approximates the solution of the incompressible Navier-Stokes equations for conservation of mass, momentum, and energy using a finite volume discretization. The flame is assumed to be axis-symmetric, time-independent, and in a state of local thermodynamic equilibrium. The chemical reactions in the jet and between the jet and the surroundings are assumed negligible. Ionization and dissociation processes are taken into account through the physical properties of the gases. The plasma is assumed to be optically thin (transparent to radiative heat transfer). The k-ε turbulence model is used with standard parameters, as in Table 1. These values are standard with no axis-symmetric correction term.[4] Swirl was not taken into ac-

Per Nylén and **Anita Hansbo,** University Trollhättan/Uddevalla, S-461 29 Trollhättan, Sweden; **Martin Friis,** Department of Solid Mechanics, Lund Institute of Technology, S-221 00 Lund, Sweden; and **Lars Pejryd,** Volvo Aero Corporation, Sweden. Contact e-mail: per@thn.htu.se.

Nomenclature

H	enthalpy	J kg^{-1}
U	axial velocity	ms^{-1}
T	temperature	K
R	nozzle radius	m
r	radius	m
R	nozzle inner radius	m
k	turbulence kinetic energy	J kg^{-1}
ϵ	turbulence dissipation rate	J kg^{-1} s^{-1}
L	mixing length	m
δ	inflow velocity width	m
C_D	drag coefficient	—
d	particle diameter	m
Re	Reynolds number	—
a	thermal accomodation coefficient	—
γ	specific heat ratio	—
Pr	Prandtl number	—
Nu	Nusslet number	—
Kn	Knudsen number	—
ν_w	molecular speed	ms^{-1}
R	universal gas constant	J mol^{-1} K^{-1}
t	time	s
q	heat flux	Wm^{-2}
h	heat transfer coefficient	Wm^{-2} K^{-1}
ϵ	radiation emissivity	—
σ	Stefan-Boltzman constant	Wm^{-2} K^{-4}
ΔH_m	latent heat of fusion	J kg^{-1}
ΔH_v	latent heat of vaporisation	J kg^{-1}
H_∞	local fluid enthalpy	J kg^{-1}
H_w	fluid enthalpy at particle surface	J kg^{-1}
Cp	specific heat	Jkg^{-1}K^{-1}
ρ	density	kg m^{-3}
k	thermal conductivity	W m^{-1} K^{-1}
μ	viscosity	kg m^{-1} s^{-1}
x	mass fraction	—
y	mass fraction	—
M	molecular weight	kg mol^{-1}

Subscripts

f	fluid phase
p	particle
w	property corresponding to wall (particle surface) temperature
∞	property corresponding to fluid temperature
m	melting
bp	boiling point

count in the simulations since it has been found to have a negligible effect.[5]

The thermodynamic and transport properties of argon, hydrogen, and air were taken from Ref 6.

Mixing rules were employed to determine the properties of the mixture (plasma + surrounding air). The specific heat (C_p) and enthalpy (H) of the mixture were calculated using mass weighted mixing rules as proposed by Bolot *et al.*[7]

$$C_p(T) = \sum_i C_{p,i}(T) x_i \quad \text{(Eq 1)}$$

$$H(T) = \sum_i H_i(T) x_i \quad \text{(Eq 2)}$$

where x stands for the mass fraction and subscript i for the argon-hydrogen and air mixture. The viscosity (μ) was calculated by the procedure described by Wilke,[8] and the thermal conductivity (k) of the mixture was calculated by the procedure described by Mason and Saxena:[9]

$$\mu(T) = \sum_i \frac{\mu_i(T)}{1 + \sum_{i \neq i} \varphi_{ij} \frac{y_j}{y_i}} \quad \text{(Eq 3)}$$

$$k(T) = \sum_i \frac{k_i(T)}{1 + \sum_{j \neq i} A_{ij} \frac{y_j}{y_i}} \quad \text{(Eq 4)}$$

where y stands for the mole fraction. The coefficients φ_{ij} and A_{ij} are dependent on the temperature and pressure, and collision integrals φ_{ij} were calculated using the Wilke approximation:[8]

$$\varphi_{ij} = \frac{1}{\sqrt{8}} \left[1 + \left(\frac{\mu_i}{\mu_j} \right)^{\frac{1}{2}} \left(\frac{M_j}{M_i} \right)^{\frac{1}{4}} \right]^2 \left[1 + \left(\frac{M_i}{M_j} \right) \right]^{-\frac{1}{2}} \quad \text{(Eq 5)}$$

where M stands for molecular weight. The coefficients A_{ij} were calculated using the Mason and Saxena's approximation:[9]

$$A_{ij} = 1.065 \varphi_{ij} \quad \text{(Eq 6)}$$

Table 1 Turbulence parameters

C_μ	C_1	C_2	Pr_t	Sc_t	ξ_{kt}	$\xi_{\epsilon t}$	ξ_{kl}	$\xi_{\epsilon l}$
0.09	1.44	1.92	0.9	0.9	1	1.3	1	1

2.1 Computational Domain and Boundary Conditions

The geometry and computational domain including the torch is illustrated in Fig. 1. The lower boundary is the symmetry axis and the flow moves toward the right. The upper and the left boundaries are open boundaries at which the temperature (300 K) and pressures (1 atm) are assumed to be constant. Since the geometry is axis-symmetric, the simulations were performed using cylindrical coordinates. The computational region, 8 cm radially and 10 cm axially, is subdivided by a nonstructured nonuniform mesh with higher densities near the torch and in regions where the highest gradients are assumed to occur. Grid sensitivity trials were made by first selecting a mesh of 2000 nodes and subsequently increasing the number of nodes by about 2000 between trials. The grid was considered sufficiently refined when two sets of computed results for two successive grid configurations differed by no more than 2 pct. The final number of nodes was 8760. The final mesh is given in Fig. 2. Torch wall temperatures were assumed to be 700 K inside and 300 K outside.

The torch inlet radial velocities were set to zero and the axial temperature (T_F) and velocity (U_F) profiles were assumed to have power law forms:

$$T_F = (T_{\max} - T_{\text{wall}})\left(1 - (r / R_{\text{inner}})^2\right) + T_{\text{wall}} \quad \text{(Eq 7)}$$

$$U_F = U_{\max}\left(1 - (r / R_{\text{inner}})^3\right) \quad \text{(Eq 8)}$$

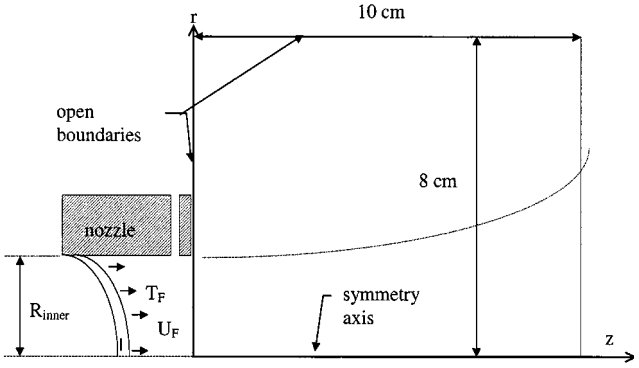

Fig. 1 The computational domain

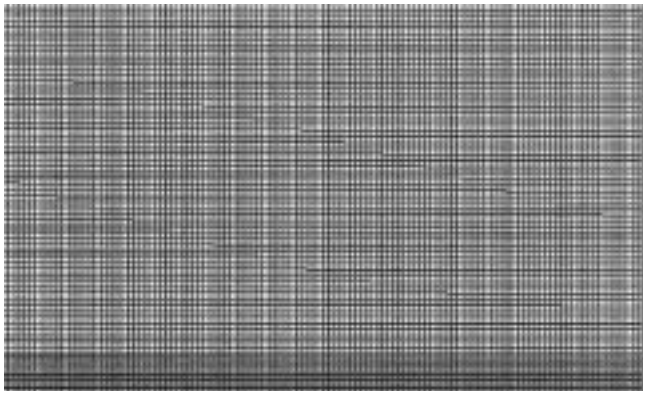

Fig. 2 Computational mesh used in the simulations

Here, r is the radial position, T_{wall} the torch wall temperature, and R_{inner} the inner radius of the nozzle. These inlet conditions are difficult to validate by measurement and other authors[5] have proposed various models (using, in particular, integer powers other than those in Eq 7 and 8). Integer values of 2 to 4 therefore were also evaluated. From this analysis, we determined that, within a reasonable range downstream from the nozzle, the results were not strongly dependent on the postulated profiles. However, a more comprehensive measurement and modeling study is needed to be able to define the most proper choice of these profiles. The terms T_{max} and U_{max} were derived from the global mass and enthalpy conservation at the nozzle exit (for the different process conditions simulated, T_{max} was typically 16 to 17000 K and U_{max} typically 1000 to 1200 m/s). The turbulence kinetic energy (k) and its dissipation rate (ε) at the inlet were specified by[5]

$$k(r) = 0.001\frac{1}{2}U_F^2 \qquad \text{(Eq 9)}$$

$$\varepsilon(r) = \frac{k^{3/2}}{L} \qquad \text{(Eq 10}$$

where

$$L = 0.075\frac{\delta}{c_\mu^{3/4}} \qquad \text{(Eq 11}$$

Here, L is the mixing length, c_μ the turbulence constant in Table 1, and δ the inflow velocity full width at tenth maximum; *i.e.*, δ is the solution of

$$U_F\left(\frac{\delta}{2}\right) = 0.1U_{max} \qquad \text{(Eq 12)}$$

The values for k and ε in Eq 9 and 10 are comparatively small, *i.e.*, assume a close to laminar flow. Although these expressions most probably lead to an underestimation of turbulence quantities in the nozzle region, we verified that the development of turbulence downstream in the jet was not significantly influenced by these choices.

3. The Two-Dimensional Particle Model

In order to calculate the particle trajectories, temperature histories, and distributions of particle impact temperatures, positions, and velocities, a two-dimensional model was used. When calculating the interactions between particles and plasma, it was assumed that the particle loading effect on the plasma is negligible (one-way coupling), *i.e.*, the presence of particles will have little effect on gas velocities and temperatures. The particle model is based on the following assumptions:

- a two-dimensional flow in which particles maintain axial and radial trajectories;
- spherical particles;
- local thermodynamic equilibrium exists;
- optically thin plasma;
- negligible gravitational effects;
- negligible effects of thermophoresis,[10] Basset history,[10] and particle charging;
- negligible turbulent effects on particle trajectories; and
- negligible vaporization effects on drag and boundary layer properties.

Based on the above assumptions, the momentum and heat transfer between the plasma and the particles can be modeled as follow.

3.1 Equations of Motion

The equation of motion of the particles is[10]

$$\frac{dU_p}{dt} = \frac{3}{4}C_D\left(U_p - U_f\right)\left|U_p - U_f\right|\frac{\rho_f}{\rho_p d_p} \qquad \text{(Eq 13)}$$

where C_{D_1} is the drag coefficient given by the following corrections as a function of the Reynolds number:[11]

$$\text{Re} = \frac{\rho_f\left|U_p - U_f\right|d_p}{\mu_f} \qquad \text{(Eq 14)}$$

$$C_{D1} = \begin{cases} 24/\mathrm{Re} & \mathrm{Re} < 0.2 \\ (24/\mathrm{Re})(1 + 0.087) & 0.2 < \mathrm{Re} < 2.0 \\ (24/\mathrm{Re})\left(1 + 0.11\,\mathrm{Re}^{0.81}\right) & 2.0 < \mathrm{Re} < 21.0 \\ (24/\mathrm{Re})\left(1 + 0.189\,\mathrm{Re}^{0.62}\right) & 21.0 < \mathrm{Re} < 500 \end{cases} \quad \text{(Eq 15)}$$

The terms ρ_f and μ_f in Eq 13 and 14 are the density and viscosity of the plasma-air mixture calculated at the bulk temperature, ρ_p the particle density, U_F the fluid velocity for the particular computational cell within which the particle resides, U_p the particle velocity, and d_p the particle diameter. The drag coefficient is corrected for noncontinuum effects by the factor[10]

$$f_1 = \left[1 + \left(\frac{2-a}{a}\right)\left(\frac{\gamma}{1+\gamma}\right)\left(\frac{4}{\mathrm{Pr}_w}\right)\mathrm{Kn}\right]^{-0.45} \quad \text{(Eq 16)}$$

where a is the thermal accommodation coefficient, γ the specific heat ratio, Pr_w the Prandtl number calculated at the particle surface temperature, and Kn the Knudsen number defined as[10]

$$\mathrm{Kn} = \frac{2\,\mathrm{Pr}_w\,\bar{k}_f}{\rho_{f,w} v_w d_p \bar{c}_p} \quad \text{(Eq 17)}$$

where the mean conductivity and specific heat are obtained by integration over the boundary layer.[13] The term $\rho_{f,w}$ is the fluid density at the wall temperature, and v_w the mean molecular speed, dependent on the molecular weight M as well as the particle surface temperature T_w:

$$v_w = \left(\frac{8RT_w}{M\pi}\right)^{1/2} \quad \text{(Eq 18)}$$

where R denotes the gas constant. The temperature of the gas drops drastically in the boundary layer, and consequently there are property variations within the boundary layer. Corrections of the drag coefficient by the factor

$$f_2 = \left(\frac{\rho_\infty \mu_f}{\rho_f \mu_\infty}\right)^{0.15} \quad \text{(Eq 19)}$$

are therefore carried out, as proposed by Lewis and Gauvin.[12] Subscripts ∞ and f in Eq 19 represent the properties at the local fluid and film temperature, respectively. The final expression for C_D becomes

$$C_D = C_{D_1} . f_1 . f_2 \quad \text{(Eq. 20)}$$

3.2 Equations of Heating

When spraying ceramics, internal heat transfer (within the particles) has to be considered.[13] The heat conduction equation may be written as[11]

$$\rho_p c_p \frac{\delta T}{\delta t} = \nabla\left(k_p(T)\nabla T\right) \quad \text{(Eq 21)}$$

In spherical coordinates, we obtain[11]

$$\rho_p c_p \frac{\delta T}{\delta t} = \frac{1}{r^2}\frac{\delta}{\delta r}\left(r^2 k_p \frac{\delta T}{\delta r}\right) \quad \text{(Eq 22)}$$

where t is the time coordinate, r is the radial coordinate within the particle, and T is the corresponding temperature. The terms ρ_p, c_p, and k_p denote the density, the specific heat, and the thermal conductivity of the particle material. The initial condition is

$$T(r,t) = T_{p_o}, t = 0,\ r \le \frac{d_p}{2} \quad \text{(Eq 23)}$$

Here, d_p is the particle diameter and T_{p_o} the temperature of the particles at the time of injection. The boundary conditions are

$$\left(\frac{\delta T}{\delta r}\right)_{r=0} = 0,\ t > 0 \quad \text{(Eq 24)}$$

$$k_p\left(\frac{\delta T}{\delta r}\right)_{r=\frac{d_p}{2}} = q,\ t > 0 \quad \text{(Eq 25)}$$

where

$$q = h\left(T_f - T_w\right) + \varepsilon\sigma\left(T_a^4 - T_w^4\right) \quad \text{(Eq 26)}$$

Here, T_f is the fluid bulk temperature for the particular computational cell within which the particle resides, T_w the particle surface temperature, ε the emmisivity, σ the Boltzman constant, and T_a the temperature far from the plasma, 300 K. As the particle traverses through the plasma flame, the particle temperature reaches the melting temperature. The heat balance at the moving solid-liquid interface is then given by

$$\Delta H_m \rho_p \frac{dr_m}{dt} = k_p\left(\frac{\delta T}{\delta t}\right)_{r=r_m} \quad \text{(Eq 27)}$$

where ΔH_m is the latent heat of fusion, r_m the radial position of the melting front, ρ_p the particle solid phase density, and k_p the liquid phase conductivity. This phase change problem is solved by the enthalpy method.[14] The heat-transfer coefficient, h, in Eq 26 is estimated using the standard convective formula[15]

$$h = \mathrm{Nu}\frac{k_f}{d_p} \quad \text{(Eq 28)}$$

where k_f is the conductivity of the plasma-air mixture at the bulk temperature and Nu is the Nusslet number calculated from the Ranz and Marshall equation.[15]

$$\mathrm{Nu}_1 = 2.0 + 0.514\,\mathrm{Re}^{0.5} \quad \text{(Eq 29)}$$

This Nusslet number is, first, corrected due to noncontinuum effects by the factor

$$f_3 = \left[1 + \left(\frac{2-a}{a}\right)\left(\frac{\gamma}{1+\gamma}\right)\left(\frac{4}{\mathrm{Pr}_{ps}}\right)\mathrm{Kn}\right]^{-1} \quad \text{(Eq 30)}$$

as proposed by Pfender and Lee,[10] and, second, due to variable properties through the boundary layer by the factor

$$f_4 = \left(\frac{\rho_\infty \mu_f}{\rho_f \mu_\infty}\right)^{0.15} \quad \text{(Eq 31)}$$

Table 2 ZrO_2 particle properties

ρ(kg m^{-3})	T_m(K)	T_{bp}(K)	ΔH_m(J kg^{-1})
5400	2950	4548	0.71e6
ΔH_v(J kg^{-1})	C_p(J kg^{-1})	k(W m^{-1} K^{-1})	Accommodation coefficient(a)
5.06×10^6	604	1.1	0.8

Table 3 The investigated factors and their high and low levels

Factor	+Level	−Level	Unit
Current	420	300	A
Argon flow rate	32	23	slpm
Hydrogen flow rate	5	3	slpm

as proposed by Lewis and Gauvain.[12] The final expression for the Nusselt number then becomes

$$\mathrm{Nu} = \mathrm{Nu}_1 \cdot f_3 \cdot f_4 \quad \text{(Eq 32)}$$

Vaporization is considered by reducing the heat transfer when the particle reaches the boiling temperature, due to the outflow of vapor; *i.e.*, q in Eq 24 is substituted by the combustion approximation[16]

$$q = \frac{\Delta H_v}{r_p} \frac{\bar{k}}{\bar{C}_p} \ln\left(1 + \frac{H_\infty - H_w}{\Delta H_v}\right) \quad \text{(Eq 33)}$$

where ΔH_v is the latent heat of vaporization, r_p the particle radius, and H_w and H_∞ denote the enthalpies at the particle surface and local fluid temperature. The gas properties for the air-plasma mixture in the boundary layer are calculated using the same mixing rules as for the plasma jet. The effect of the particle vapors on the plasma properties is not considered. The axial injection location was randomly generated by sampling from a uniform distribution between −2 and −4 mm upstream from the nozzle exit (internal injection). The mean of the particle injection velocity was set to 13 m/s, and the particle size distribution was taken from the sieve analysis and is given in Ref 1.

4. Experimental

The experimental procedure has already been described in the companion article (Part I, *cf.* Ref 1). However, a brief description is provided here for completeness.

4.1 Materials

A commercially available powder, 7.7% yttria partially stabilized zirconia produced by H.C. Starck (Gostar, Germany) as Amperit 827 was used in this study. The particle properties used in the simulations are given in Table 2.

4.2 Plasma Spraying

Plasma spraying was carried out using the SM-F-100 Connex (Wohlen, Switzerland) gun. The gun was controlled by an automated and robotized Sultzer Metco (Wohlen, Switzerland) A3000 air plasma unit. The powder was injected radially internally 3 mm upstream from the nozzle exit.

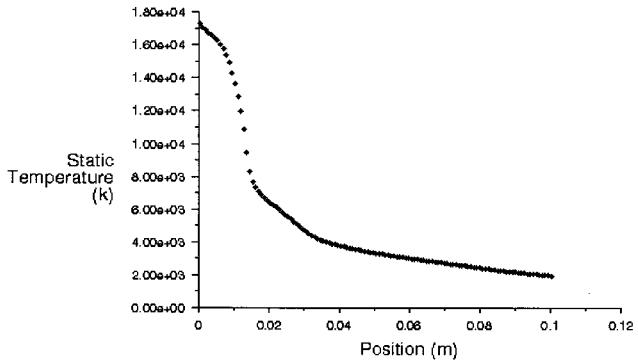

Fig. 3 Plasma centerline temperature profile (K)

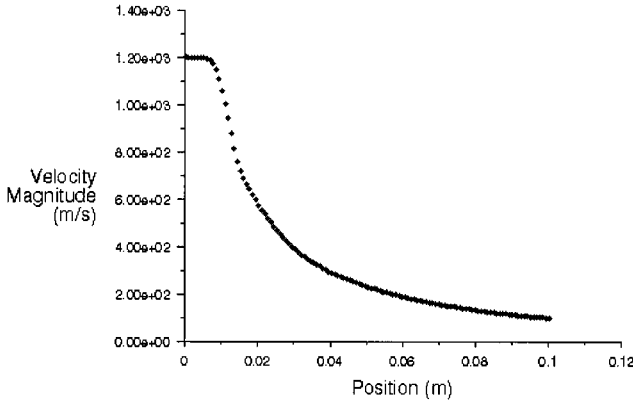

Fig. 4 Plasma centerline velocity profile (m/s)

4.3 The Diagnostics of In-Flight Sprayed Particles

The diagnostics of in-flight sprayed particles were measured using the optical system DPV2000, developed by the National Research Council of Canada (Industrial Materials Institute, Boucherville, PQ, Canada) and Tecnar Automation Ltée (St Hubert, PQ, Canada). The properties were measured 70 mm from the nozzle exit in the center of the particle flux.[1]

4.4 The Simulations

The simulations were performed using a CCF statistical design. This design was selected since it gives information about the curvature of the particle property function. The assumed linear parameter-property relationship in Ref 1 therefore could be validated. The parameters and their levels are given in Table 3. These are the same as in the statistical investigation,[1] except that the powder mass flow rate has been excluded, as the model neglects the particle loading effect.

5. Results and Discussion

The centerline decay of jet temperature and velocity is shown in Fig. 3 and 4. There is a noticeable change in the slope in both the temperature and velocity curves at approximately 10 mm from the nozzle exit.

Table 4 Simulation design matrix and predicted and measured (in parentheses) average particle properties 70 mm downstream from nozzle exit

Ar (slpm)	H_2 (slpm)	Current (A)	Temperature (K)	Velocity (m/s)
23	3	300	3084 (3352)	113 (114)
32	3	300	2925 (3280)	123 (118)
23	5	300	3151 (3365)	118 (115)
32	5	300	2957 (3300)	124 (124)
23	3	420	3815 (3477)	167 (138)
32	3	420	3220 (3404)	172 (143)
23	5	420	3858 (3512)	176 (146)
32	5	420	3304 (3461)	172 (155)
23	4	360	3415	136
32	4	360	3024	139
27.5	3	360	3240	154
27.5	5	360	3206	139
27.5	4	300	2978	120
27.5	4	420	3497	175
27.5	4	360	3262	151
27.5	4	360	3268	152
27.5	4	360	3260	152

The torch efficiency was measured on one occasion to 52% and considered to be independent of the spray parameters. The voltage was noticed to be sensitive to the hydrogen flow rate. Measured averages were 43, 46, and 49 V for the respective hydrogen 3, 4, and 5 slpm flow rates. Investigated parameters, predicted average particle velocities, and temperatures are given in Table 4. The corresponding measured properties[1] are given in parentheses.

It should be noticed that the measurements represent the property averages in the center of the particle flux, while the predictions correspond to all particles passing the plane 70 mm downstream from the nozzle exit. The overall agreement is fairly good, albeit the velocities are overestimated for the 420 A cases and the temperatures are underestimated in the 300 A cases. This discrepancy might be due to the method chosen to correct the Nusslet number in Eq 29. Several other methods have been proposed.[11] When comparing measurements and predictions, it was of particular interest whether the model presented was able to predict correct trends when operating conditions were varied. A mean least regression (MLR) analysis of the predictions therefore was made, using the Modde software system (Umetri AB, Umeå, Sweden). In order to make a transparent comparison, only the first eight rows in Table 4 were used. The measured and predicted changes in respective response when the factors are changed within their ranges are given in Fig. 5. Only the main effects have been included in these figures. The trends are in good agreement, but the effects are generally overestimated.

In the experimental investigation,[1] we determined a local linear approximation to the response function (particle velocity and temperature) in the neighborhood of the tests. Since the statistical design in this paper (*cf.* Table 4) includes center points, it is possible to fit a second-order polynomial in the least-squares sense. Consequently, the curvature of the response function can be estimated. In Fig. 6, prediction plots are given, representing the change in the responses when the current varies over its range. Similar plots, where the hydrogen and argon flow rates were varied, revealed that the assumed linear parameter-property relationship[1] is appropriate; *i.e.*, a two-level statistical design seems sufficient within the selected ranges.

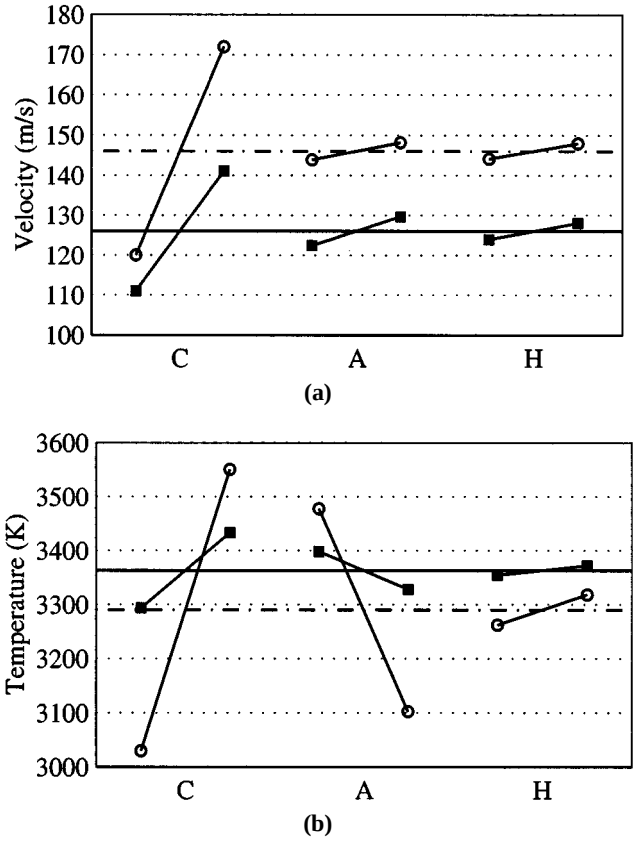

Fig. 5 Predicted and measured effects of the respective factors when each factor is varied within its ranges. The black squares correspond to the measured effects, whereas the circles correspond to the predicted effects.

To be able to control the particle in-flight characteristics online or to optimize spraying conditions of a powder, a fast computational model is needed. If model predictions can be used to obtain such relationships, the need of expensive experiments is reduced. Independent regressions of average particle velocity and temperature yielded the following equations (Eq 34 and 35) (based on all the predictions in Table 4). Only statistically significant terms have been included.

$$\text{Velocity} = C + a \times \text{Ar} + b \times I \quad \text{(Eq 34)}$$

$$\text{Temperature} = C + a \times \text{Ar} + b \times I + c \times \text{H}_2 + d \times Ar \times I \quad \text{(Eq 35)}$$

where the coefficients *C, a, b, c,* and d are given in Table 5. The Ar, *I,* and H_2 represent the argon mass flow rate, current, and the hydrogen mass flow rate coded to -1 to 1. The term R^2 in Table 5 represents the fraction of the variation of the response explained by the model, and Q^2 represents the fraction of the response that can be predicted by the model.[3] The R^2 and Q^2 values close to 1 are indicative of the model's quality and efficiency. The predictions in Table 4 can be well described by Eq 34 and 35, since both R^2 and Q^2 are larger than 0.9.

Yielded regression contour plots for unmelted fraction of particles and average particle velocities are given in Fig. 7. The unmelted fraction of particles was calculated as the particle number

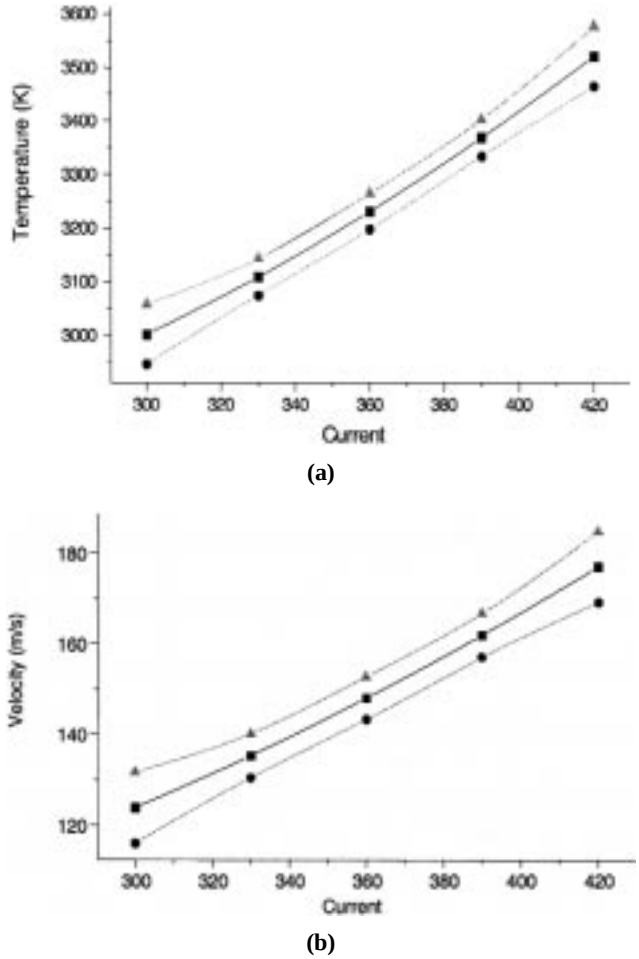

Fig. 6 Predicted average particle (**a**) temperatures (K) and (**b**) velocities (m/s) when the current is varied over its ranges. The upper and lower curves represent a 90% confidence interval

Table 5 Yielded coefficients, explanation degree (R_2), and predictability (Q_2) in the regression analysis

	Velocity coefficients	Temperature coefficients
C (constant)	146.059	3261.882
a	2.1	−189.3
b	26.5	18
c	…	259.9
d	…	−99.5
Q_2	0.919	0.9594
R_2	0.9411	0.9824

fraction that had a surface temperature below the melting point (2950 K). Alternatively, the core temperature or the individual ratio unmelted of each particle could have been used instead.

The response contours in Fig. 7 can be superimposed to determine optimal parameter settings, for instance, to minimize the fraction of unmelted particles while simultaneously maximizing the average velocity. This would represent the upper left corner in Fig. 7, *i.e.*, a 23 slpm argon mass flow rate and a 420 A current. However, a larger number of particles, than the present 300 in each simulation, should probably be used to give a more certain value of the fraction of unmelted particles.

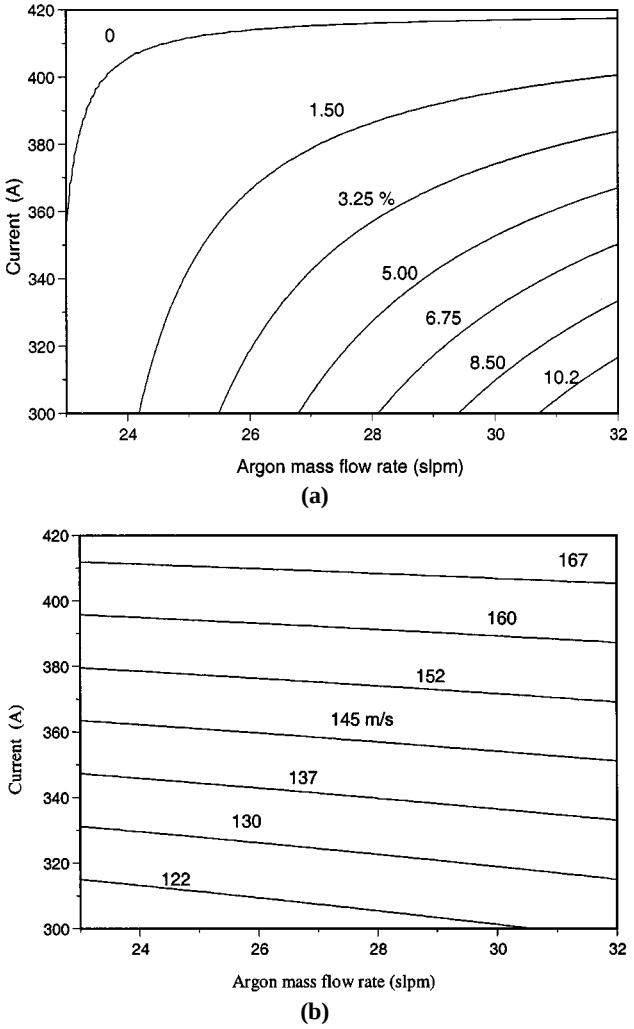

Fig. 7 Contour plot for (**a**) unmelted fraction of particles (%) and (**b**) average particle velocity (m/s) where the argon flow rate (slpm) and current (A) have been varied. The hydrogen flow rate = 4 slpm.

6. Conclusions

In this article, a mathematical model of the atmospheric pressure plasma spray process has been described. The influence of arc current and primary and secondary gas flows on particle in-flight properties has been systematically studied. The results show reasonably good agreement with measurements and the model seems capable of predicting correct trends when operation conditions are varied. The most significant factor in both experiments and simulations was the current. The predicted particle temperature and velocity was also expressed in terms of spray gun parameters. Such relationships can be useful in on-line control and in numerical optimization of the plasma spray process. The ability to yield regression equations from the fluid dynamic simulations looks promising. However, the model has to be refined since it overestimates the effects when process parameters are varied. Specifically, the particle temperatures are overestimated. More sophisticated models to calculate nozzle exit conditions as well as heat-transfer coefficients between jets

and particles might increase model accuracy. Further work on these subjects is planned.

Acknowledgments

This work was supported by Stiftelsen för Kunskaps och Kompetensutveckling, Project No. 1996/654.

References

1. M. Friis, P. Nylén J. Wigrén, and C. Persson: *J. Thermal Spray Technol.*, 2001, vol. 10 (2).
2. C. Moreau, P. Gougeon, M. Lamontagne, V. Lacasse, G. Vaudreuil, and P. Cielo: in *Thermal Spray: Industrial Applications*, C.C. Berndt and S. Sampath, eds., ASM International, Materials Park, OH, 1994, pp. 431-37.
3. *Modde Reference Manual*, Umetri AB, Umeå, Sweden.
4. B.E. Launder and D.B. Spalding: *Appl. Mech. Eng.*, 1974, No. 3, pp. 269-89.
5. C.H. Chang, J.D. Ramshaw, Numerical Simulations of Argon Plasma Jets Flowing into Cold Air, Plasma Chemistry and Plasma Processing, Vol. 13, No. 2, 1993, pp. 189-209.
6. P. Boulos, P. Fauchais, and E. Pfender: *Thermal Plasmas: Fundamentals and Applications*, Plenum Publishing Corp., New York, NY, 1994, vol. I.
7. R. Bolot, M. Imbert, and C. Coddet: in *Thermal Spray: A United Forum for Scientific and Technological Advances*, C.C. Berndt, ed., ASM International, Materials Park, OH, 1997, pp. 549-55.
8. C.R. Wilke: *J. Chem. Phys.*, 1950, vol. 18 (4), pp. 517-19.
9. E.A. Mason and S.C. Saxena: *Phys. Fluids*, 1958, vol. 1 (5), pp. 361-69.
10. E. Pfender and Y.C. Lee: *Plasma Chem. Processing*, 1985, vol. 5 (3), pp. 211-37.
11. *Plasma Spraying Theory and Applications*, R. Suryanarayanan, ed., World Scientific Publishing, Singapore, 1993.
12. J.A. Lewis and W.H. Gauvin: *AIChE J.*, 1973, vol. 19, pp. 982-90.
13. E. Bourdin, P. Fauchais, and M. Boulos: *Int. J. Heat Mass Transfer*, 1983, vol. 26, pp. 567-82.
14. V. Voller and M. Cross: Accurate Solution on Moving Boundary Problem Using the Enthalpy Method, *Int. J. Heat and Mass Transfer*, 1981,vol. 24, pp. 749-756.
15. Frank P. Incropera, David P. De Witt: *Fundamentals of Heat and Mass Transfer*, John Wiley & Sons, New York, NY, 1990.
16. M.K. Wu, J.S. McFeaters, B.J. Welch, and R.L. Stephens: *Trans. IChemE*, 1991, vol. 69A, pp. 21-24.